Mechanical and chemical activation of GPR68 (OGR1) probed with a genetically-encoded fluorescent reporter

Alper D Ozkan[1], Tina Gettas[1], Audrey Sogata[2], Wynn Phaychanpheng[2], Miou Zhou[1], and Jérôme J Lacroix[1*]

[1]Graduate College of Biomedical Sciences, Western University of Health Sciences, 309 E. Second St, Pomona, CA 91766

[2]Chino Hills High School, 16150 Pomona Rincon Rd, Chino Hills, CA 91709

***corresponding author** Dr. Jerome J. Lacroix

Western University of Health Sciences

309 E. Second St, Pomona, CA 91766

Tel: 909-469-8201

Email: jlacroix@westernu.edu

Key-words: mechanobiology, GPCR, fluid shear stress, genetically-encoded fluorescent reporter

Summary statement

This study introduces a genetically-encoded fluorescent reporter sensitive to known mechanical and chemical activators of GPR68, a mechanosensitive G-protein coupled receptor involved in vascular, neural, and immune functions.

Abstract

G-protein coupled receptor (GPCR) 68 (GPR68, or OGR1) couples extracellular acidifications and mechanical stimuli to G-protein signaling and plays important roles in vascular physiology, neuroplasticity, and cancer progression. Inspired by previous GPCR-based reporters, here, we inserted a cyclic permuted fluorescent protein into the third intracellular loop of GPR68 to create a genetically-encoded fluorescent reporter of GPR68 activation we call "iGlow". iGlow responds to known physiological GPR68 activators such as fluid shear stress and extracellular acidifications. In addition, iGlow responds to Ogerin, a synthetic GPR68-selective agonist, but not to a non-active Ogerin analog, showing the specificity of iGlow-mediated fluorescence signals. Flow-induced iGlow activation is not eliminated by pharmacological modulation of downstream G-protein signaling, disruption of actin filaments, or application of GsMTx4, an inhibitor of certain mechanosensitive ion channels activated by membrane stretch. Deletion of the conserved Helix 8, proposed to mediate mechanosensitivity in certain GPCRs, does not eliminate flow-induced iGlow activation. iGlow could be useful to investigate the contribution of GPR68-dependent signaling in health and disease.

Introduction

G-protein coupled receptors (GPCRs) constitute the largest known family of membrane receptors, comprising at least 831 human homologs organized into 6 functional classes (A to F). They play essential roles in a wide range of biological functions spanning all major physiological systems including olfaction, energy homeostasis and blood pressure regulation. They also control embryonic development and tissue remodeling in adults. The biological significance of GPCRs is underscored by the fact that ~13% of all known human GPCRs represent the primary targets of

~34% of all pharmaceutical interventions approved by the Food and Drug Administration (Hauser, Chavali et al., 2018).

GPCRs possess a conserved structure encompassing seven transmembrane helices and switch between resting and active conformations depending on the presence of specific physico-chemical stimuli. In addition to recognizing a vast repertoire of small molecules, such as odorants, hormones, cytokines, and neurotransmitters, some GPCRs sense physico-chemical signals, including photons (Filipek, Stenkamp et al., 2003), ions (Strasser, Wittmann et al., 2015), membrane depolarizations (Barchad-Avitzur, Priest et al., 2016; Ben-Chaim, Chanda et al., 2006; Birk, Rinne et al., 2015; Rinne, Mobarec et al., 2015; Vickery, Machtens et al., 2016) and mechanical forces (Chachisvilis, Zhang et al., 2006; Storch, Mederos y Schnitzler et al., 2012; Wei, Bianchi et al., 2018; Xu, Mathur et al., 2018). Once activated, GPCRs physically interact with heterotrimeric G-proteins (Gα, Gβ and Gγ), promoting the exchange of guanosine diphosphate (GDP) for guanosine triphosphate (GTP) on the Gα subunit. This process, called G-protein engagement, enables the GTP-bound Gα subunit and the Gβγ complex to dissociate from their receptor and activate downstream cellular effectors.

GPCRs often recognize more than one stimulus and interact with one or more Gα proteins amongst 18 known homologs, enabling them to finely tune downstream biological responses to a complex stimulus landscape (Syrovatkina, Alegre et al., 2016). One example of a GPCR sensing multiple stimuli and triggering pleiotropic G-protein signaling is GPR68, a class-A GPCR first identified in an ovarian cancer cell line and hence initially named ovarian cancer G-protein coupled Receptor 1, or OGR1 (Xu and Casey, 1996). GPR68 is expressed in a surprisingly large number of tissues (Regard, Sato et al., 2008; Xu, Mathur et al., 2018) and is often up-regulated in many types of cancers (Wiley, Sriram et al., 2019; Xu, Mathur et al., 2018).

Although sphingophosphorylcholine lipids were proposed to act as endogenous GPR68 ligands (Mogi, Tomura et al., 2005; Xu, Zhu et al., 2000), it is now well-established that GPR68 is physiologically activated by extracellular protons (Ludwig, Vanek et al., 2003), a property shared with only three other GPCRs to date (GPR4, GPR65 and GPR132). As reported for several GPCRs, GPR68 is also activated by endogenous mechanical stimuli, such as fluid shear stress and membrane stretch (Erdogmus, Storch et al., 2019; Wei, Bianchi et al., 2018; Xu, Mathur et al., 2018). Importantly, this mechanosensitivity seemingly enables GPR68 to mediate flow-induced dilation in small-diameter arteries (Xu, Mathur et al., 2018). GPR68 can engage $G\alpha_{q/11}$, which increases cytosolic concentration of calcium ions ($[Ca^{2+}]_{cyt}$) through phospholipase C-β (PLC-β), as well as $G\alpha_{s}$, which increases the production of cyclic adenosine monophosphate (cAMP) through adenylate cyclase activation.

The synthetic GPR68 agonist Ogerin increases pH-dependent cAMP production by GPR68 but reduces pH-dependent calcium signals, suggesting Ogerin acts as a biased positive allosteric modulator of GPR68 (Huang, Karpiak et al., 2015). Interestingly, Ogerin suppresses recall in fear conditioning in wild-type but not $GPR68^{-/-}$ mice, suggesting a role of GPR68 in learning and memory (Huang, Karpiak et al., 2015). Hence, although the contribution of GPR68 to vascular physiology has been relatively well-established, its role in other organs remains unclear.

A genetically-encoded fluorescent reporter of GRP68 activation would help bridge this gap. GPCR activation is often monitored using Fluorescence Resonance Energy Transfer (FRET) or Bioluminescence Resonance Energy Transfer (BRET) (Angers, Salahpour et al., 2000; Chachisvilis, Zhang et al., 2006; Erdogmus, Storch et al., 2019). However, FRET necessitates complex measurements to separate donor and acceptor emissions whereas BRET often requires

long integration times and sensitive detectors to capture faint signals. In contrast, recent reporters engineered by fusing GPCRs with a cyclic permuted green fluorescent protein (cpGFP) have enabled robust and rapid *in vitro* and *in vivo* detection of GPCR stimuli including dopamine (Patriarchi, Cho et al., 2018; Sun, Zeng et al., 2018), acetylcholine (Jing, Zhang et al., 2018), norepinephrine (Feng, Zhang et al., 2019), and serotonin (Dong, Ly et al., 2021) using simple intensity-based fluorescence measurements. Here, we borrowed a similar cpGFP-based engineering approach to create a genetically-encodable reporter of GPR68 stimuli. We call it indicator of GPR68 stimuli by flow and low pH, or iGlow.

Results

iGlow responds to flow

We designed iGlow by borrowing a protein engineering design from previously developed GPCR-based fluorescent reporters containing cpGFP. In cpGFP, the N- and C- termini are relocated to a β-sheet, locally disrupting the integrity of the β-barrel whose main function is to shield the proteinogenic chromophore from collisions with solvent molecules. Circular permutation thus makes cpGFP fluorescence sensitive to the conformation of its N- and C-termini (Nasu, Shen et al., 2021). Large fluorescence changes are hence anticipated to occur when cpGFP is inserted via its N- and C- termini into the third intracellular loop of GPCRs, a region known to undergo large conformational rearrangement upon stimulus-mediated activation (Rasmussen, DeVree et al., 2011). We generated iGlow by genetically translocating the cpGFP module taken from the voltage-indicator ASAP1 (St-Pierre, Marshall et al., 2014), which was originally obtained from GCaMP3 (Tian, Hires et al., 2009), and inserting it into the third intracellular loop of human GPR68. We then flanked cpGFP with the genetically-optimized N-

terminal (LSSLI) and C-terminal (NHDQL) linkers from the dopamine sensor dLight1.2, designed by fusing cpGFP into the third intracellular loop of the dopamine receptor DRD1 (Patriarchi, Cho et al., 2018) (**Figure 1A, Supplementary Figure 1 and Supplementary Table 1**).

To explore the sensitivity of iGlow to fluid flow, a physiological stimulus of GPR68, we first co-transfected HEK293T cells with two plasmids, one encoding iGlow and the other encoding a cytosolic red fluorescent protein mCherry. Transfected cells were seeded onto microscope-compatible flow chambers and exposed to fluid shear stress (FSS) by circulating Hank's Balanced Salt Solution (HBSS, pH 7.3) using a computer-controlled peristaltic pump while green and red fluorescence were recorded simultaneously using split imaging optics mounted on an inverted epifluorescence microscope (flow-induced shear stress was calibrated according to the flow chamber manufacturer's instructions, see **Supplementary Figure 2**). Cells were stimulated with a discontinuous FSS stimulation protocol (10 sec on, 10 sec off) in which the amplitude of FSS pulses was incrementally increased. This protocol produced robust and transient increases in green, but not red, fluorescence intensity, suggesting that the transient change in green emission intensity did not result from imaging artifacts which would have equally affected both fluorescence channels (**Figure 1B**).

In iGlow, as in other engineered GPCR-based reporters, the cpGFP module is located near the lipid bilayer. One cannot thus exclude the possibility that some molecular components embedded or associated with the cell membrane (e.g., lipids, membrane proteins, cytoskeletal elements…) could physically collide with cpGFP when the membrane is exposed to flow. Such hypothetical molecular collisions might induce cpGFP barrel distortions, causing changes in fluorescence emission. If that were the case, all or part of the fluorescence signals observed in

Figure 1B could occur independently of stimulus-induced conformational rearrangements of the linkers connecting GPR68 to cpGFP. One way to determine the contribution of linker-independent cpGFP barrel distortions to flow-induced iGlow fluorescence signals is to evaluate flow-induced fluorescence responses of cpGFP inserted into a non-mechanosensitive membrane protein at a position near the membrane, i.e., similar to how cpGFP in iGlow is located near the lipid bilayer. The presence of mechanically-evoked fluorescence signals in such a construct would indicate that iGlow might respond to flow in a linker-independent manner. To test this possible scenario, we tested two cpGFP-containing membrane proteins that are not known (or anticipated) to exhibit mechanosensitivity: the voltage indicator ASAP1 (St-Pierre, Marshall et al., 2014) and Lck-cpGFP, a cpGFP fused to the myristoylated and palmitoylated N-terminal domain of the lymphocyte-specific kinase (Lck) (Shigetomi, Kracun et al., 2010). In ASAP1, cpGFP is located extracellularly, whereas in Lck-cpGFP, cpGFP is located intracellularly (**Figure 1C**). Nevertheless, in both constructs cpGFP is located in the vicinity of the lipid bilayer and thus these constructs would seem valid to test our hypothesis that cpGFP fluorescence may be modulated by membrane components. Upon application of our intermittent flow protocol, no fluorescence change other than normal photobleaching decay occurred, even upon high flow conditions (> 10 dyne cm^{-2}). These results confirm that the fluorescence signals mediated by iGlow are not likely to be contributed by linker-independent barrel distortion of cpGFP and are rather likely produced as a result of conformational changes propagated from the GPR68 core to the cpGFP chromophore in a linker-dependent manner (**Figure 1D-E**).

We next determined the dynamic range of iGlow fluorescence by exposing cells to single FSS pulses ranging from 1.3 to 20.8 dynes cm^{-2} (**Figure 1F**). We used the amplitude of the fluorescence peaks, calculated as max $\Delta F/F_0$, to quantify the amount of iGlow activation. The peak amplitude gradually increases over the tested shear stress range, the largest being a nearly 3-fold increase between 10.4 and 20.8 dynes cm^{-2} (approximately 25% to 75%), which matches well the dynamic range of GPR68 activation measured with calcium imaging (Xu, Mathur et al., 2018) (**Figure 1G**). In addition, the delay between mechanical stimulation and peak fluorescence (time to peak) was negatively correlated with the amplitude of the FSS pulses (Pearson's correlation coefficient = -0.77), stronger pulses producing shorter time to peak values. The relationship between pulse amplitude and time to peak is not linear and was best fitted by an exponential function (R^2 = 0.81, red trace in **Figure 1H**). Next, we performed a multiple-pulse protocol with 1 min interval between each pulse to measure the repeatability of iGlow signals. Our data indicate that, although subsequent pulses induce subsequent fluorescence peaks, the amplitude of subsequent peaks tend to be lower than the first one (**Figure 1I**).

From our epifluorescence imaging data, we noticed that, in some cells, both baseline iGlow fluorescence (i.e., before stimulation) and FSS-induced signals appear to originate not only from the plasma membrane, but also from within the cell, whereas in other cells, these signals tend to be localized at the cell periphery consistent with cell surface localization (**Figure 1J**). We investigated the cellular localization of iGlow with higher spatial resolution using confocal microscopy. To this aim, HEK293T cells were co-transfected with two plasmids, one encoding iGlow and the other encoding a red fluorescent marker of actin (LifeAct-mScarlet), or a red fluorescent protein tagged with a C-terminal CAAX domain (dsRed-CAAX and HcRed-CAAX) which enables trafficking of RAS proteins to cell membranes (Michaelson, Ali et al.,

2005). Live-cell confocal fluorescence imaging shows that, whereas iGlow baseline fluorescence appears to localize near or at the cell surface, a more diffuse fluorescence can also be seen throughout some cells (**Figure 2**).

iGlow senses chemical GPR68 activators

Next, we investigated the ability of iGlow to activate upon application of the GPR68-selective agonist Ogerin and extracellular acidifications. First, we acutely perfused iGlow-expressing cells with HBSS as a vehicle control, or HBSS containing 10 µM Ogerin or 10 µM of a non-active Ogerin analog (Huang, Karpiak et al., 2015). Compared to vehicle control, application of Ogerin leads to transient iGlow activation with large max $\Delta F/F_0$ values (Dunn's multiple comparisons test p-value = 0.0067) whereas application of the non-active analog yielded no significant signal (Dunn's multiple comparisons test p-value > 0.9999) (**Figure 3A-D**). To assess the optical dynamic range of iGlow, we compared iGlow signals with those produced by cells expressing dLight1.2 and acutely exposed to 10 µM dopamine (dopa). As expected, dLight1.2 produces robust responses to dopamine, the maximal amplitude of which were not significantly different than the responses of iGlow to Ogerin (Dunn's multiple comparisons test p-value > 0.9999). The time to peak values of Ogerin-induced iGlow signals were also significantly shorter when stimulating iGlow with 10 µM Ogerin as compared to a strong FSS pulse of 20.8 dyne cm^{-2} (Mann-Whitney U-test p-value = 0.0307) (**Figure 3D**).

We next perfused iGlow-expressing cells with an acidic physiological solution, decreasing extracellular pH from 7.3 to 6.5, or with a vehicle control maintaining a neutral external pH. iGlow produced robust and transient signals that were larger at pH 6.5 (Mann-Whitney U-test p-value = 0.0034) (**Figure 4A-B**). In few cells, iGlow also responded so some

degree to the vehicle control. We interpret this response by the fact that iGlow might be partially activated by the shear stress produced by rapidly exchanging solution in the culture vessel. To reduce the amount of baseline activation prior measurement, we next increased external pH to 8.2 (Xu, Mathur et al., 2018) and applied a single FSS pulse of 2.6 dyne cm^{-2} using a physiological solution at pH 8.2 (n = 28), 7.3 (n = 24) or 6.5 (n = 10), (**Figure 4C**). Our data show that flow-evoked iGlow signals tend to be larger at pH 6.5 vs. pH 8.2 (Tukey's multiple comparisons test p-value = 0.0155) (**Figure 4D-E**). In line with the effect of extracellular acidifications on signal amplitude, the mean time to peak value was also significantly shorter at pH 6.5 vs. to 8.2 (Tukey's multiple comparisons test p-value = 0.0261) (**Figure 4F**).

Flow-induced iGlow activation is independent of G-proteins

To test if iGlow signals depend on specific interactions between GPR68 and regulatory cytoplasmic proteins, we stimulated iGlow with a 2.6 dyne cm^{-2} FSS pulse in cells pre-treated with one of several pharmacological agents. We used GTP-γ-S, a non-hydrolyzable GTP analog which prevents Gα protein association to GPCRs; NF449, a GDP→GTP exchange inhibitor which selectively prevents $G\alpha_s$ dissociation from its receptor (Hohenegger, Waldhoer et al., 1998); and BIM-46187, a non-specific GDP→GTP exchange Gα inhibitor (Ayoub, Damian et al., 2009). We also tested CMPD101, an inhibitor of G-protein receptor kinases 2/3 (GRK2/3) (**Figure 5A**). Most treatments did not significantly change the mean peak fluorescence nor the time to peak values (**Figure 5B-D**). One exception was GTP-γ-S treatment, which imparted a significant increase in mean max $\Delta F/F_0$ from 66 ± 6 % (control) to 100 ± 9 % (Dunnett's multiple comparisons test p-value = 0.0044).

Unlike its parent receptor DRD1, dLight1.2 cannot trigger downstream G-protein signaling (Patriarchi, Cho et al., 2018). Consistent with this study, we found that dLight1.2 signals were not significantly affected by any of our pharmacological treatments (one-way ANOVA p-value = 0.5441) (**Supplementary Figure 3**). To determine whether iGlow exhibits an analogous loss of downstream signaling due to cpGFP insertion, we stimulated cells with extracellular protons (pH 6.5) and measured calcium responses by monitoring fluorescence from the red calcium indicator JRGECO1a (Dana, Mohar et al., 2016) **(Figure 5E)**. Co-transfecting cells with a WT GPR68-encoding plasmid significantly increased calcium-dependent fluorescent responses (Dunnett's multiple comparisons test p-value = 0.0248), whereas transecting cells with iGlow did not (Dunnett's multiple comparisons test p-value = 0.9943), suggesting a loss of iGlow-mediated downstream signaling through the $G\alpha_{q/11}$ pathway.

Flow-induced iGlow activation is resilient

We next sought to determine whether iGlow signals depend on the integrity of the actin cytoskeleton. To this aim, we transfected HEK293T cells with LifeAct-mScarlet to monitor real-time actin disorganization upon treatment with 20 µM cytochalasin D (CD20), an inhibitor of actin polymerization. Actin filaments were completely disorganized after 20 min (**Figure 6A**). Since we observed visible cell death upon one-hour 20 µM CD treatment, we monitored iGlow's response to FSS immediately after a 20 min CD incubation. At the shear amplitude of 2.6 dyne cm^{-2}, iGlow produced fluorescence signals similar to untreated cells, even upon increasing CD concentration to 50 µM CD (one-way ANOVA p-value = 0.6825) (**Figure 6B-C**). These results

show that, at this shear stress amplitude, the integrity of the actin cytoskeleton is not required for shear stress sensing by iGlow.

Acute incubation with micromolar concentrations of the small spider toxin GsMTx4 inhibits activation of certain mechanosensitive ion channels by membrane stretch, fluid shear stress and mechanical indentation (Alcaino, Knutson et al., 2017; Bae, Sachs et al., 2011; Jetta, Gottlieb et al., 2019; Li, Xu et al., 2019; Suchyna, Tape et al., 2004). In addition, GsMTx4 also reduces the activity of the membrane motor Prestin (Fang and Iwasa, 2006), an essential component of the cochlear amplifier of outer hair cells (Dallos and Fakler, 2002; Zheng, Shen et al., 2000). Given the apparent large inhibition spectrum of GsMTx4 on mechanotransduction membrane proteins, we wondered whether GsMTx4 could also inhibit iGlow. We first performed a positive control experiments by measuring Ca^{2+} entry mediated by the GsMTx4-sensitive mechanosensitive Piezo1 channel in response to a 2.6 dyne cm^{-2} pulse in the presence or absence of 2.5 µM GsMTx4 (Bae, Sachs et al., 2011). We monitored intracellular free Ca^{2+} ions by co-transfecting PIEZO1-deficient cells (Dubin, Murthy et al., 2017) with a mouse Piezo1 plasmid and a plasmid encoding the fluorescent calcium indicator GCaMP6f (Chen, Wardill et al., 2013). Our data show that this toxin concentration was able to reduce GCaMP6f fluorescence response (max $\Delta F/F_0$) from +75 ± 5 % to +16 ± 2 %, a nearly 5-fold reduction (Student's T-test p-value = 9.7×10^{-18}) (**Figure 6D-E**). In contrast, the same treatment did not significantly affect the amplitude of iGlow signals induced by a 2.6 dyne cm^{-2} pulse (Student's T-test p-value = 0.9116) (**Figure 6F-G**).

Class-A GPCRs harbor a structurally-conserved amphipathic helical motif located immediately after the seventh transmembrane segment, called helix 8. A recent study showed that deletion of helix 8 abolished mechanical, but not ligand-mediated, activation in the histamine receptor H1R (Erdogmus, Storch et al., 2019). Furthermore, transplantation of H1R helix 8 into a mechano-insensitive GPCR was sufficient to confer mechanosensitivity to the chimeric receptor (Erdogmus, Storch et al., 2019). The online tool NetWheels indicates that GPR68 also contains an amphipathic helical motif resembling the helix 8 of H1R (**Supplementary Figure 4**). We introduced a non-sense codon (TGA) to eliminate this motif and the remainder of the C-terminal region from iGlow (**Supplementary Figure 1**) and tested the sensitivity of the deletion mutant, H8Del, to a single FSS pulse of 2.6 dyne cm^{-2}. At this shear stress amplitude, the mean peak amplitude produced by H8Del was not statistically different than those produced by the full-length iGlow (Student's T-test p-value = 0.3933) (**Figure 6H-I**). In addition, the time to peak was similar in both cases (Student's T-test p-value = 0.8808) (**Figure 6J**). These results show that helix 8 is not required for shear flow activation by iGlow. Since the C-terminal deletion may have eliminated regulatory sites involved in GPCR desensitization, H8Del could enable repeated stimulations with less signal loss compared to iGlow. When H8Del was stimulated with a 1.7 dynes cm^{-2} pulse every minute, the peak amplitude remained relatively constant for the first four peaks with less signal loss than iGlow (**Figure 6K-L**). To determine whether H8Del senses shear stress when expressed in other cells, we transfected this construct into HEK293T cells and Chinese Hamster Ovary (CHO-K1) cells and stimulated these cells with a 2.6 dynes cm^{-2} pulse of 10 s duration. The mean response of H8Del was not significantly different in both cell types (Student's T test p-value = 0.2519) (**Supplementary Figure 5)**.

We next transiently expressed iGlow *in vivo* under the control of an astrocyte-specific promoter by stereotaxically injecting adeno-associated viruses into the hippocampal CA3 region of mice. The choice of this injection site was motivated by several studies indicating endogenous expression of GPR68 in the brain (Xu, Mathur et al., 2018), including the hippocampus (Regard, Sato et al., 2008), whereas the choice of the promoter was motivated by the expression of GPR68 in reactive astrocytes (Schneider, Goetsch et al., 2012). Using confocal microscopy on acute hippocampal slices, robust green fluorescence was visible in the CA3 region, while adjacent brain regions had minimal fluorescence, suggesting iGlow could, in the future, be expressed in a spatially-defined manner for *in vivo* detection of GPR68-stimuli (**Supplementary Figure 6**).

Discussion

This study introduces iGlow, a genetically-encoded fluorescent sensor of GPR68 activation. iGlow responds to all currently known activators of GPR68, i.e. fluid shear stress, the synthetic agonist Ogerin and extracellular acidifications. More importantly, iGlow does not respond to an inactive ogerin analog (Huang, Karpiak et al., 2015). Given the high structural similarity between these compounds (the sole difference being the orientation of the benzyl alcohol relative to the triazin ring), this selectivity suggests iGlow retains the endogenous structure of the GPR68 receptor and the ability of GPR68 to functionally discriminate two structurally similar ligands. In contrast to dLight1.2, the cellular localization of iGlow appears not strictly confined to the plasma membrane. We do not know if this reflects endogenous trafficking of GPR68 or partial degradation or misfolding due to the presence of cpGFP in iGlow. Alkalinization has been shown to induce internalization of GPR68 in leukocytes (Tan, Yamaguchi et al., 2018). Such

physiological regulation of GPR68 location might, at least in part, contribute to the formation of an intracellular pool of iGlow. Future studies will be needed to investigate this possibility.

Another unexpected property of iGlow is the relatively large cell-to-cell fluctuations of the overall fluorescence time course in response to the same flow stimulus. These fluctuations may reflect the intrinsic heterogeneity of morphologies and mechanical properties of cultured cells which may lead to heterogenous flow-induced mechanical stress and thus heterogenous iGlow activation profiles. Despite these fluctuations, the peak amplitude of iGlow fluorescence signals was, on average, larger and occurred quicker when the amplitude of tested physiological stimuli (shear stress and external protons) was larger.

A potential advantage of iGlow is its insensitivity to pharmacological modulation of G-protein signaling, disruption of actin cytoskeleton, and incubation with GsMTx4, a toxin proposed to inhibit certain mechanosensitive ion channels by partitioning into the lipid bilayer, effectively "buffering" the effect of shear stress and/or membrane stretch (Gnanasambandam, Ghatak et al., 2017). As in dLight1.2, the insertion of the cpGFP module near the G-protein binding site apparently uncouples iGlow from G-protein signaling, allowing the reporter to function as an ‘observer’ that does not perturb endogenous signaling. However, the lack of signal elimination by cytochalasin D and GsMTx4 treatments is more puzzling since numerous mechanosensitive ion channels show at least partial reduction of mechanosensitivity in response to these treatments (Alcaino, Knutson et al., 2017; Bae, Sachs et al., 2011; Gottlieb, Bae et al., 2012; Hurst, Gottlieb et al., 2009; Jia, Ikeda et al., 2016; Kamaraju, Gottlieb et al., 2010; Nishizawa and Nishizawa, 2007; Ostrow, Mammoser et al., 2003; Shen, Wong et al., 2015).

To date, mechanosensitivity has been reported in at least one class-B GPCR (parathyroid hormone type 1 receptor) (Zhang, Frangos et al., 2009) and many class-A subfamilies including A3 (bradykinin receptor B2, Apelin receptor and angiotensin II type 1 receptor) (Chachisvilis, Zhang et al., 2006; Kwon, Wang et al., 2016; Mederos y Schnitzler, Storch et al., 2008), A6 (vasopressin receptor 1A) (Mederos y Schnitzler, Storch et al., 2008), A13 (sphingosine receptor 1) (Jung, Obinata et al., 2012), A15 (GPR68) (Wei, Bianchi et al., 2018; Xu, Mathur et al., 2018), A17 (dopamine receptor DRD5) (Abdul-Majeed and Nauli, 2011) and A18 (muscarinic receptor M5R and histamine receptor H1R) (Erdogmus, Storch et al., 2019; Mederos y Schnitzler, Storch et al., 2008). Helix 8 is both necessary and sufficient to confer mechanosensitivity in certain class-A GPCRs such as H1R (Erdogmus, Storch et al., 2019). However, helix 8 is not necessary for flow-induced iGlow activation. In addition, while mechanical activation is independent from ligand-mediated activation in some class-A GPCRs (Erdogmus, Storch et al., 2019), the deletion of five histidine residues (H17, H20, H84, H169, and H269) abrogate both pH-sensing and flow-sensing in GPR68, suggesting the binding of protons is required for GPR68 mechanosensitivity (Ludwig, Vanek et al., 2003; Xu, Mathur et al., 2018). Hence, GPR68 and iGlow may sense both stimuli using a non-canonical helix-8 independent pathway. Further investigations will be necessary to identify underlying mechanisms of mechanosensitivity.

To conclude, iGlow probes GPR68 activation by endogenous and exogenous stimuli and should be useful to determine the biological roles of GPR68 in vascular and non-vascular physiology, such as hippocampal plasticity.

Methods

Molecular cloning

A fragment containing the human GPR68 cDNA was obtained by digesting a pBFRT-GPR68 plasmid (a gift from Drs. Mikhail Shapiro, Caltech and Ardèm Patapoutian, Scripps Research) by NdeI and BamHI. The insert was ligated into an in-house pCDNA3.1-Lck-GCaMP6f plasmid linearized by the same enzymes, creating the plasmid pCDNA3.1-GPR68. A cpGFP cassette was amplified by PCR from a pCDNA3.1 plasmid encoding ASAP1, a gift from Dr. Michael Lin, Stanford, available as Addgene #52519 and inserted into pCDNA3.1-GPR68 using the NEBuilder HiFi DNA Assembly kit (New England Biolabs). The pCNDA3.1-jRGECO1a plasmid was cloned by assembling PCR-amplified fragments from pGP-CMV-NES-jRGECO1a, Addgene # 61563, a gift from Dr. Douglas Kim (Dana, Mohar et al., 2016) and pCDNA3.1. All constructs were confirmed by Sanger sequencing (GENEWIZ). The pLifeAct-mScarlet-N1 plasmid was obtained from Addgene #85054, a gift from Dr. Dorus Gadella (Bindels, Haarbosch et al., 2017). The DsRed-CAAX and HcRed-CAAX plasmids were a gift from Dr. Bradley Andersen. All molecular biology reagents were purchased from New England Biolabs.

Cell culture, transfection, and drug treatment

HEK293T and CHO-K1 cells were obtained from the American Tissue Culture Collection and ΔPZ1 cells were a gift from Ardèm Patapoutian (Scripps Research). Cells were not recently authenticated nor tested for contamination. Cells were cultured in standard conditions (37 °C, 5 % CO_2) in a Dulbecco's Modified Eagle's Medium supplemented with Penicillin (100 U mL^{-1}), streptomycin (0.1 mg mL^{-1}), 10 % sterile Fetal Bovine Serum, 1X Minimum Essential Medium non-essential amino-acids and without L-glutamine. All cell culture products were purchased

from Sigma-Aldrich. Plasmids were transfected in cells (passage number < 35) seeded in 96-well plates at ~50 % confluence 2-4 days before the experiment with FuGene6 (Promega) or Lipofectamine 2000 (Thermo Fisher Scientific) and following the manufacturer's instructions. 1-2 days before experiments, cells were gently detached by 5 min incubation with Phosphate Buffer Saline and re-seeded onto 18 mm round glass coverslips (Warner Instruments) or onto disposable flow chambers (Ibidi µ-slides 0.4mm height), both coated with Matrigel (Corning). Cells were treated with each drug at 15 min (CMPD101), 20 min (cytochalasin D and NF449), 30 min (GTP-gamma-S and GsMTx4) or 2 hrs (BIM-46187) prior to measurement. pH-shear experiments were performed using a starting pH of 8.2, adjusted 15 min prior to measurement. CMPD101 (#5642) and NF-449 (#1391) were purchased from R&D Systems (Biotechne), GTP-gamma-S was purchased from Cytoskeleton, Inc (#BS01), Dopamine (#H8502) and Gαq inhibitor BIM-46187 (#5332990001) were purchased from Sigma-Aldrich.

Fluorescence imaging

Excitation light of desired wavelengths were produced by a Light Emitting Diode light engine (Spectra X, Lumencor), cleaned through individual single-band excitation filters (Semrock) and sent to the illumination port of an inverted fluorescence microscope (IX73, Olympus) by a liquid guide light. Excitation light was reflected towards a plan super apochromatic 100X oil-immersion objective with a 1.4 numerical aperture (Olympus) using a triple-band dichroic mirror (FF403/497/574, Semrock). Emission light from the sample was filtered through a triple-band emission filter (FF01-433/517/613, Semrock) and sent through beam-splitting optics (W-View Gemini, Hamamatsu). Split and unsplit fluorescence images were collected by a sCMOS camera (Zyla 4.2, ANDOR, Oxford Instruments). Spectral separation by the Gemini was done using flat

imaging dichroic mirrors and appropriate emission filters (Semrock). Images were collected by the Solis software (ANDOR, Oxford Instruments) at a rate of 1 frame s^{-1} through a 10-tap camera link computer interface. Image acquisition and sample illumination were synchronized using TTL triggers digitally generated by the Clampex software (Molecular Devices). To reduce light-induced bleaching, samples were only illuminated for 200 ms, i.e. during frame acquisition (200 ms exposure). To reduce auto-fluorescence, the cell culture medium was replaced with phenol red-free HBSS approximately 20 min prior experiments. Due to the narrow field of view at this magnification, only 1-3 transfected cells were measured per each flow assay.

Image analyses

A MATLAB script (available to download at Open Science Framework, see below) was used to calculate the average fluorescence intensity of each cell of interest at each frame, expressed as percentile above the fluorescence at t = 0 ("deltaF/F"). Prior to analysis, photobleaching was corrected using the exponential fit method and a "mask" (.jpg format) separating cells of interest from the background was manually drawn in ImageJ. This mask, in addition to a bleach-corrected image sequence (.tif format) corresponding to each frame of the video, is read by the MATLAB script. The output of the script is a text file containing "deltaF/F" values at each frame for each cell in the mask ("bleachcorrected.txt", rows and columns correspond to frame ID and individual cells respectively), and a figure showing the original image, the mask, and deltaF/F traces for each cell ("figure.jpg"). Backgrounds are either removed manually in ImageJ, or within the MATLAB script by taking the average fluorescence intensity of all non-cell pixels and subtracting this value from the intensity values associated with cells at each frame.

AAV production, hippocampal injection, and brain imaging

All animal procedures followed the Institutional Animal Care and Use Committee of the Western University of Health Sciences. Brain-optimized adeno-associated viruses PHP.eB (Chan, Jang et al., 2017) (AAV-PHP.eB) harboring iGlow under transcriptional control by the GFAP promoter (GFAP-iGlow-WPRE AAV-PHP.eB) were produced by VectorBuilder. To express iGlow in the CA1 pyramidal fields of the hippocampus, high titers of GFAP-iGlow-WPRE AAV-PHP.eB virus (0.7 µl, $1x10^{13}$ genome copies per ml) were stereotaxically injected into the hippocampal CA1 sub region of 3-month-old male C57Bl/6N mice through a glass micropipette at 4 sites at the following coordinates relative to bregma (mm): AP: -1.8, ML: ±0.8, DV: -1.6; or AP: -2.5, ML: ±2, DV: -1.6). After injection, the micropipette was left in place for an additional 5-min to ensure full virus diffusion. After surgery, mice were treated with antibiotics and their health was monitored every day for 2 weeks. For brain slice imaging, mice were euthanized by isoflurane inhalation and their brain dissected and chilled in ice-cold artificial cerebrospinal fluid (aCSF) containing the following (in mM): 124 NaCl, 2.5 KCl, 1.25 NaH2PO4, 24 NaHCO3, 2 ascorbic acid, 10 glucose, 1.5 MgSO4, and 2.5 CaCl2, bubbled with 95% O2 and 5% CO2. Hippocampal slices (0.35 mm thick) were obtained using a McIlwain tissue chopper as previously described (Zhou and Baudry, 2006). After isolation, hippocampal slices were placed in incubation baskets in aCSF saturated with 95% O2–5% CO2 and incubated for one 1 h recovery period at room temperature. Slices were next transferred to petri dishes and place under a confocal microscope (Zeiss LSM 880). Standard GFP settings were used to image iGlow.

Fluid shear stress stimulation and calculations

Fluid shear-stress stimulation was done by circulating extracellular physiological solutions at various speeds into µ-slide channels (Ibidi) using a Clampex-controlled peristaltic pump (Golander). In order to accurately determine the amplitude of shear stress applied inside the flow chambers, we compared shear stress values determined by multiplying the average flow-rate by a coefficient provided by the manufacturer (**see Supplementary Figure 2**).

Statistical analyses

The number n represents the number of independent cells or cell clusters analyzed. To evaluate pairwise differences of mean data sets, we performed Mann-Whitney U-tests when $n \leq 10$ and Student's T-tests when $n > 10$ in both data sets. For comparing means of more than two groups, Dunnett's or Tukey's multiple comparisons tests were performed following one-way ANOVA when $n \geq 10$ in each group, whereas Dunn's multiple comparisons tests were performed following one-way Kruskal-Wallis analysis of variance when $n < 10$ in at least one group. All error bars are standard errors of the mean. Statistical tests were performed using OriginPro 2018, GraphPad Prism 8.2, or a Mann-Whitney online calculator.

Data availability

Data obtained from fluorescence traces ($\Delta F/F_0$ and time to peak values) and our MATLAB script have been deposited in the Open Science Framework (OSF) public Depository (DOI 10.17605/OSF.IO/8MP4W).

Acknowledgments

We thank Ardèm Patapoutian for the gift of the human GPR68 cDNA and Bradley Andresen for help with confocal imaging.

Competing interests

No competing interests declared

Funding

This work was supported by intramural and start-up funds from Western University of Health Sciences (to J.J.L), federal work-study (to T.G) and National Institutes of Health (GM130834 and NS101384 to J.J.L).

References

Abdul-Majeed, S., and Nauli, S. M. (2011). Dopamine receptor type 5 in the primary cilia has dual chemo- and mechano-sensory roles. *Hypertension*. **58**:325-331.

Alcaino, C., Knutson, K., Gottlieb, P. A., Farrugia, G., and Beyder, A. (2017). Mechanosensitive ion channel Piezo2 is inhibited by D-GsMTx4. *Channels (Austin)*. **11**:245-253.

Angers, S., Salahpour, A., Joly, E., Hilairet, S., Chelsky, D., Dennis, M., and Bouvier, M. (2000). Detection of beta 2-adrenergic receptor dimerization in living cells using bioluminescence resonance energy transfer (BRET). *Proc. Natl. Acad. Sci. U. S. A.* **97**:3684-3689.

Ayoub, M. A., Damian, M., Gespach, C., Ferrandis, E., Lavergne, O., De Wever, O., Baneres, J. L., Pin, J. P., and Prevost, G. P. (2009). Inhibition of heterotrimeric G protein signaling by a small molecule acting on Galpha subunit. *J. Biol. Chem.* **284**:29136-29145.

Bae, C., Sachs, F., and Gottlieb, P. A. (2011). The mechanosensitive ion channel Piezo1 is inhibited by the peptide GsMTx4. *Biochemistry*. **50**:6295-6300.

Barchad-Avitzur, O., Priest, M. F., Dekel, N., Bezanilla, F., Parnas, H., and Ben-Chaim, Y. (2016). A Novel Voltage Sensor in the Orthosteric Binding Site of the M2 Muscarinic Receptor. *Biophys. J.* **111**:1396-1408.

Ben-Chaim, Y., Chanda, B., Dascal, N., Bezanilla, F., Parnas, I., and Parnas, H. (2006). Movement of 'gating charge' is coupled to ligand binding in a G-protein-coupled receptor. *Nature*. **444**:106-109.

Bindels, D. S., Haarbosch, L., van Weeren, L., Postma, M., Wiese, K. E., Mastop, M., Aumonier, S., Gotthard, G., Royant, A., Hink, M. A., and Gadella, T. W., Jr. (2017). mScarlet: a bright monomeric red fluorescent protein for cellular imaging. *Nat. Methods*. **14**:53-56.

Birk, A., Rinne, A., and Bunemann, M. (2015). Membrane Potential Controls the Efficacy of Catecholamine-induced beta1-Adrenoceptor Activity. *J. Biol. Chem.* **290**:27311-27320.

Chachisvilis, M., Zhang, Y. L., and Frangos, J. A. (2006). G protein-coupled receptors sense fluid shear stress in endothelial cells. *Proc. Natl. Acad. Sci. U. S. A.* **103**:15463-15468.

Chan, K. Y., Jang, M. J., Yoo, B. B., Greenbaum, A., Ravi, N., Wu, W. L., Sanchez-Guardado, L., Lois, C., Mazmanian, S. K., Deverman, B. E., and Gradinaru, V. (2017). Engineered AAVs for efficient noninvasive gene delivery to the central and peripheral nervous systems. *Nat. Neurosci.* **20**:1172-1179.

Chen, T. W., Wardill, T. J., Sun, Y., Pulver, S. R., Renninger, S. L., Baohan, A., Schreiter, E. R., Kerr, R. A., Orger, M. B., Jayaraman, V., Looger, L. L., Svoboda, K., and Kim, D. S. (2013). Ultrasensitive fluorescent proteins for imaging neuronal activity. *Nature*. **499**:295-300.

Dallos, P., and Fakler, B. (2002). Prestin, a new type of motor protein. *Nat. Rev. Mol. Cell Biol.* **3**:104-111.

Dana, H., Mohar, B., Sun, Y., Narayan, S., Gordus, A., Hasseman, J. P., Tsegaye, G., Holt, G. T., Hu, A., Walpita, D., Patel, R., Macklin, J. J., Bargmann, C. I., Ahrens, M. B., Schreiter, E. R., Jayaraman, V., Looger, L. L., Svoboda, K., and Kim, D. S. (2016). Sensitive red protein calcium indicators for imaging neural activity. *Elife*. **5**.

Dong, C., Ly, C., Dunlap, L. E., Vargas, M. V., Sun, J., Hwang, I. W., Azinfar, A., Oh, W. C., Wetsel, W. C., Olson, D. E., and Tian, L. (2021). Psychedelic-inspired drug discovery using an engineered biosensor. *Cell*.

Dubin, A. E., Murthy, S., Lewis, A. H., Brosse, L., Cahalan, S. M., Grandl, J., Coste, B., and Patapoutian, A. (2017). Endogenous Piezo1 Can Confound Mechanically Activated Channel Identification and Characterization. *Neuron*. **94**:266-270 e263.

Erdogmus, S., Storch, U., Danner, L., Becker, J., Winter, M., Ziegler, N., Wirth, A., Offermanns, S., Hoffmann, C., Gudermann, T., and Mederos, Y. S. M. (2019). Helix 8 is the essential structural motif of mechanosensitive GPCRs. *Nat Commun*. **10**:5784.

Fang, J., and Iwasa, K. H. (2006). Effects of tarantula toxin GsMTx4 on the membrane motor of outer hair cells. *Neurosci. Lett.* **404**:213-216.

Feng, J., Zhang, C., Lischinsky, J. E., Jing, M., Zhou, J., Wang, H., Zhang, Y., Dong, A., Wu, Z., Wu, H., Chen, W., Zhang, P., Zou, J., Hires, S. A., Zhu, J. J., Cui, G., Lin, D., Du, J., and Li, Y. (2019). A Genetically Encoded Fluorescent Sensor for Rapid and Specific In Vivo Detection of Norepinephrine. *Neuron*. **102**:745-761 e748.

Filipek, S., Stenkamp, R. E., Teller, D. C., and Palczewski, K. (2003). G protein-coupled receptor rhodopsin: a prospectus. *Annu. Rev. Physiol.* **65**:851-879.

Gnanasambandam, R., Ghatak, C., Yasmann, A., Nishizawa, K., Sachs, F., Ladokhin, A. S., Sukharev, S. I., and Suchyna, T. M. (2017). GsMTx4: Mechanism of Inhibiting Mechanosensitive Ion Channels. *Biophys. J.* **112**:31-45.

Gottlieb, P. A., Bae, C., and Sachs, F. (2012). Gating the mechanical channel Piezo1: a comparison between whole-cell and patch recording. *Channels (Austin)*. **6**:282-289.

Hauser, A. S., Chavali, S., Masuho, I., Jahn, L. J., Martemyanov, K. A., Gloriam, D. E., and Babu, M. M. (2018). Pharmacogenomics of GPCR Drug Targets. *Cell*. **172**:41-54 e19.

Hohenegger, M., Waldhoer, M., Beindl, W., Boing, B., Kreimeyer, A., Nickel, P., Nanoff, C., and Freissmuth, M. (1998). Gsalpha-selective G protein antagonists. *Proc. Natl. Acad. Sci. U. S. A.* **95**:346-351.

Huang, X. P., Karpiak, J., Kroeze, W. K., Zhu, H., Chen, X., Moy, S. S., Saddoris, K. A., Nikolova, V. D., Farrell, M. S., Wang, S., Mangano, T. J., Deshpande, D. A., Jiang, A., Penn, R. B., Jin, J., Koller, B. H., Kenakin, T., Shoichet, B. K., and Roth, B. L. (2015). Allosteric ligands for the pharmacologically dark receptors GPR68 and GPR65. *Nature*. **527**:477-483.

Hurst, A. C., Gottlieb, P. A., and Martinac, B. (2009). Concentration dependent effect of GsMTx4 on mechanosensitive channels of small conductance in E. coli spheroplasts. *Eur. Biophys. J.* **38**:415-425.

Jetta, D., Gottlieb, P. A., Verma, D., Sachs, F., and Hua, S. Z. (2019). Shear stress-induced nuclear shrinkage through activation of Piezo1 channels in epithelial cells. *J. Cell Sci.* **132**.

Jia, Z., Ikeda, R., Ling, J., Viatchenko-Karpinski, V., and Gu, J. G. (2016). Regulation of Piezo2 Mechanotransduction by Static Plasma Membrane Tension in Primary Afferent Neurons. *J. Biol. Chem.* **291**:9087-9104.

Jing, M., Zhang, P., Wang, G., Feng, J., Mesik, L., Zeng, J., Jiang, H., Wang, S., Looby, J. C., Guagliardo, N. A., Langma, L. W., Lu, J., Zuo, Y., Talmage, D. A., Role, L. W., Barrett, P. Q., Zhang, L. I., Luo, M., Song, Y., Zhu, J. J., and Li, Y. (2018). A genetically encoded fluorescent acetylcholine indicator for in vitro and in vivo studies. *Nat. Biotechnol.* **36**:726-737.

Jung, B., Obinata, H., Galvani, S., Mendelson, K., Ding, B. S., Skoura, A., Kinzel, B., Brinkmann, V., Rafii, S., Evans, T., and Hla, T. (2012). Flow-regulated endothelial S1P receptor-1 signaling sustains vascular development. *Dev. Cell*. **23**:600-610.

Kamaraju, K., Gottlieb, P. A., Sachs, F., and Sukharev, S. (2010). Effects of GsMTx4 on bacterial mechanosensitive channels in inside-out patches from giant spheroplasts. *Biophys. J.* **99**:2870-2878.

Kwon, H. B., Wang, S., Helker, C. S., Rasouli, S. J., Maischein, H. M., Offermanns, S., Herzog, W., and Stainier, D. Y. (2016). In vivo modulation of endothelial polarization by Apelin receptor signalling. *Nat Commun*. **7**:11805.

Li, H., Xu, J., Shen, Z. S., Wang, G. M., Tang, M., Du, X. R., Lv, Y. T., Wang, J. J., Zhang, F. F., Qi, Z., Zhang, Z., Sokabe, M., and Tang, Q. Y. (2019). The neuropeptide GsMTx4 inhibits a mechanosensitive BK channel through the voltage-dependent modification specific to mechano-gating. *J. Biol. Chem.* **294**:11892-11909.

Ludwig, M. G., Vanek, M., Guerini, D., Gasser, J. A., Jones, C. E., Junker, U., Hofstetter, H., Wolf, R. M., and Seuwen, K. (2003). Proton-sensing G-protein-coupled receptors. *Nature*. **425**:93-98.

Mederos y Schnitzler, M., Storch, U., Meibers, S., Nurwakagari, P., Breit, A., Essin, K., Gollasch, M., and Gudermann, T. (2008). Gq-coupled receptors as mechanosensors mediating myogenic vasoconstriction. *EMBO J.* **27**:3092-3103.

Michaelson, D., Ali, W., Chiu, V. K., Bergo, M., Silletti, J., Wright, L., Young, S. G., and Philips, M. (2005). Postprenylation CAAX processing is required for proper localization of Ras but not Rho GTPases. *Mol. Biol. Cell*. **16**:1606-1616.

Mogi, C., Tomura, H., Tobo, M., Wang, J. Q., Damirin, A., Kon, J., Komachi, M., Hashimoto, K., Sato, K., and Okajima, F. (2005). Sphingosylphosphorylcholine antagonizes proton-sensing ovarian cancer G-protein-coupled receptor 1 (OGR1)-mediated inositol phosphate production and cAMP accumulation. *J. Pharmacol. Sci.* **99**:160-167.

Nasu, Y., Shen, Y., Kramer, L., and Campbell, R. E. (2021). Structure- and mechanism-guided design of single fluorescent protein-based biosensors. *Nat. Chem. Biol.* **17**:509-518.

Nishizawa, M., and Nishizawa, K. (2007). Molecular dynamics simulations of a stretch-activated channel inhibitor GsMTx4 with lipid membranes: two binding modes and effects of lipid structure. *Biophys. J.* **92**:4233-4243.

Ostrow, K. L., Mammoser, A., Suchyna, T., Sachs, F., Oswald, R., Kubo, S., Chino, N., and Gottlieb, P. A. (2003). cDNA sequence and in vitro folding of GsMTx4, a specific peptide inhibitor of mechanosensitive channels. *Toxicon*. **42**:263-274.

Patriarchi, T., Cho, J. R., Merten, K., Howe, M. W., Marley, A., Xiong, W. H., Folk, R. W., Broussard, G. J., Liang, R., Jang, M. J., Zhong, H., Dombeck, D., von Zastrow, M., Nimmerjahn, A., Gradinaru, V., Williams, J. T., and Tian, L. (2018). Ultrafast neuronal imaging of dopamine dynamics with designed genetically encoded sensors. *Science*. **360**.

Rasmussen, S. G., DeVree, B. T., Zou, Y., Kruse, A. C., Chung, K. Y., Kobilka, T. S., Thian, F. S., Chae, P. S., Pardon, E., Calinski, D., Mathiesen, J. M., Shah, S. T., Lyons, J. A., Caffrey, M., Gellman, S. H., Steyaert, J., Skiniotis, G., Weis, W. I., Sunahara, R. K., and Kobilka, B. K. (2011). Crystal structure of the beta2 adrenergic receptor-Gs protein complex. *Nature*. **477**:549-555.

Regard, J. B., Sato, I. T., and Coughlin, S. R. (2008). Anatomical profiling of G protein-coupled receptor expression. *Cell*. **135**:561-571.

Rinne, A., Mobarec, J. C., Mahaut-Smith, M., Kolb, P., and Bunemann, M. (2015). The mode of agonist binding to a G protein-coupled receptor switches the effect that voltage changes have on signaling. *Sci Signal*. **8**:ra110.

Schneider, J. W., Goetsch, S. C., Leng, X., Ludwig, S. M., Russell, J. L., Yang, C. P., and Zhang, Q. J. (2012). Coupling hippocampal neurogenesis to brain pH through proneurogenic small molecules that regulate proton sensing G protein-coupled receptors. *ACS Chem. Neurosci.* **3**:557-568.

Shen, B., Wong, C. O., Lau, O. C., Woo, T., Bai, S., Huang, Y., and Yao, X. (2015). Plasma membrane mechanical stress activates TRPC5 channels. *PLoS One*. **10**:e0122227.

Shigetomi, E., Kracun, S., and Khakh, B. S. (2010). Monitoring astrocyte calcium microdomains with improved membrane targeted GCaMP reporters. *Neuron Glia Biol.* **6**:183-191.

St-Pierre, F., Marshall, J. D., Yang, Y., Gong, Y., Schnitzer, M. J., and Lin, M. Z. (2014). High-fidelity optical reporting of neuronal electrical activity with an ultrafast fluorescent voltage sensor. *Nat. Neurosci.* **17**:884-889.

Storch, U., Mederos y Schnitzler, M., and Gudermann, T. (2012). G protein-mediated stretch reception. *Am J Physiol Heart Circ Physiol*. **302**:H1241-1249.

Strasser, A., Wittmann, H. J., Schneider, E. H., and Seifert, R. (2015). Modulation of GPCRs by monovalent cations and anions. *Naunyn Schmiedebergs Arch. Pharmacol.* **388**:363-380.

Suchyna, T. M., Tape, S. E., Koeppe, R. E., 2nd, Andersen, O. S., Sachs, F., and Gottlieb, P. A. (2004). Bilayer-dependent inhibition of mechanosensitive channels by neuroactive peptide enantiomers. *Nature*. **430**:235-240.

Sun, F., Zeng, J., Jing, M., Zhou, J., Feng, J., Owen, S. F., Luo, Y., Li, F., Wang, H., Yamaguchi, T., Yong, Z., Gao, Y., Peng, W., Wang, L., Zhang, S., Du, J., Lin, D., Xu, M., Kreitzer, A. C., Cui, G., and Li, Y. (2018). A Genetically Encoded Fluorescent Sensor Enables Rapid and Specific Detection of Dopamine in Flies, Fish, and Mice. *Cell*. **174**:481-496 e419.

Syrovatkina, V., Alegre, K. O., Dey, R., and Huang, X. Y. (2016). Regulation, Signaling, and Physiological Functions of G-Proteins. *J. Mol. Biol.* **428**:3850-3868.

Tan, M., Yamaguchi, S., Nakamura, M., and Nagamune, T. (2018). Real-time monitoring of pH-dependent intracellular trafficking of ovarian cancer G protein-coupled receptor 1 in living leukocytes. *J. Biosci. Bioeng.* **126**:363-370.

Tian, L., Hires, S. A., Mao, T., Huber, D., Chiappe, M. E., Chalasani, S. H., Petreanu, L., Akerboom, J., McKinney, S. A., Schreiter, E. R., Bargmann, C. I., Jayaraman, V., Svoboda, K., and Looger, L. L. (2009). Imaging neural activity in worms, flies and mice with improved GCaMP calcium indicators. *Nat. Methods*. **6**:875-881.

Vickery, O. N., Machtens, J. P., Tamburrino, G., Seeliger, D., and Zachariae, U. (2016). Structural Mechanisms of Voltage Sensing in G Protein-Coupled Receptors. *Structure*. **24**:997-1007.

Wei, W. C., Bianchi, F., Wang, Y. K., Tang, M. J., Ye, H., and Glitsch, M. D. (2018). Coincidence Detection of Membrane Stretch and Extracellular pH by the Proton-Sensing Receptor OGR1 (GPR68). *Curr. Biol.* **28**:3815-3823 e3814.

Wiley, S. Z., Sriram, K., Salmeron, C., and Insel, P. A. (2019). GPR68: An Emerging Drug Target in Cancer. *Int. J. Mol. Sci.* **20**.

Xu, J., Mathur, J., Vessieres, E., Hammack, S., Nonomura, K., Favre, J., Grimaud, L., Petrus, M., Francisco, A., Li, J., Lee, V., Xiang, F. L., Mainquist, J. K., Cahalan, S. M., Orth, A. P., Walker, J. R., Ma, S., Lukacs, V., Bordone, L., Bandell, M., Laffitte, B., Xu, Y., Chien, S., Henrion, D., and Patapoutian, A. (2018). GPR68 Senses Flow and Is Essential for Vascular Physiology. *Cell*. **173**:762-775 e716.

Xu, Y., and Casey, G. (1996). Identification of human OGR1, a novel G protein-coupled receptor that maps to chromosome 14. *Genomics*. **35**:397-402.

Xu, Y., Zhu, K., Hong, G., Wu, W., Baudhuin, L. M., Xiao, Y., and Damron, D. S. (2000). Sphingosylphosphorylcholine is a ligand for ovarian cancer G-protein-coupled receptor 1. *Nat. Cell Biol.* **2**:261-267.

Zhang, Y. L., Frangos, J. A., and Chachisvilis, M. (2009). Mechanical stimulus alters conformation of type 1 parathyroid hormone receptor in bone cells. *Am. J. Physiol. Cell Physiol.* **296**:C1391-1399.

Zheng, J., Shen, W., He, D. Z., Long, K. B., Madison, L. D., and Dallos, P. (2000). Prestin is the motor protein of cochlear outer hair cells. *Nature*. **405**:149-155.

Zhou, M., and Baudry, M. (2006). Developmental changes in NMDA neurotoxicity reflect developmental changes in subunit composition of NMDA receptors. *J. Neurosci.* **26**:2956-2963.

Figures

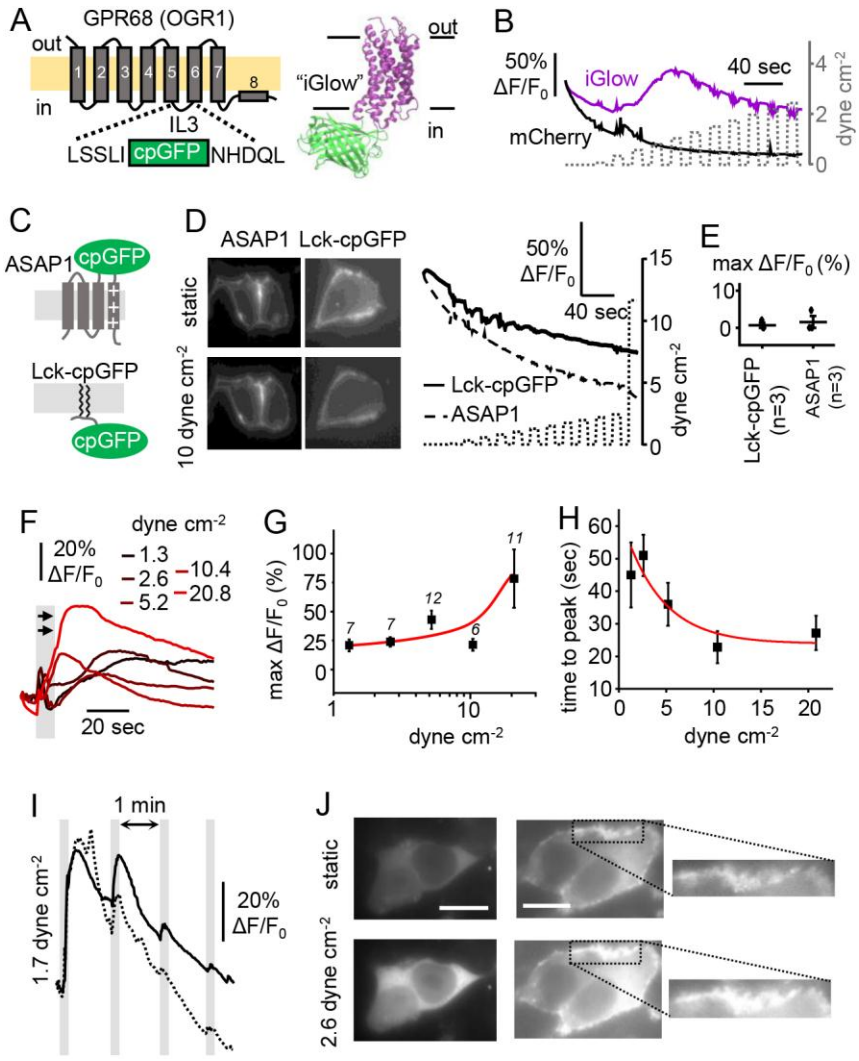

Figure 1: Design and characterization of iGlow. (**A**) *Left:* iGlow was designed by inserting cpGFP (green) into the third intracellular loop (IL3) of GPR68 (purple). *Right:* structural model of iGlow generated using the Molecular Operating Environment (MOE) software from the crystal structure of cpGFP (PDBID: 3O77, green) and a structural model of GPR68 (purple) generated by Huang et al. (Huang, Karpiak et al., 2015). (**B**) Fluorescence time-courses from a cell co-transfected with a plasmid encoding iGlow (purple trace) and a plasmid encoding a

soluble mCherry (black trace) in response to intermittent shear stress pulses (10 sec on, 10 sec off) of incrementally-increased amplitudes. (**C**) Cartoons showing the position of cpGFP in ASAP1 and Lck-cpGFP. (**D**) *Left*: epifluorescence images of cells expressing ASAP1 or Lck-cpGFP under static of flow conditions. *Right*: example of fluorescence time-courses from cells expressing ASAP1 (dashed line) or Lck-cpGFP (solid line) in response to FSS pulses of incrementally increased amplitudes (dotted line). (**E**) Scatter plots showing the maximal ΔF/F0 values obtained with ASAP1 (n = 3) and Lck-cpGFP (n = 3) using the same FSS protocol as in (D). (**F**) iGlow fluorescence signals evoked by single shear stress pulses (grey bar) of indicated amplitude. (**G**) Maximal $\Delta F/F_0$ values produced by iGlow as a function of the FSS pulse amplitude. Numbers above data indicate the number of independent replicates. Red line = trend line. (**H**) Time to peak values plotted as function of the shear stress amplitude. Red line = mono-exponential fit ($R^2 = 0.81$). (**I**) Fluorescence time course from two independent iGlow expressing cells (solid and dashed lines) obtained with repeated shear stress pulse (1.7 dyne cm^{-2}) with 1 min recovery. (**J**) Epifluorescence images showing iGlow fluorescence in static or flow condition (scale bar = 10 μm). In panels (E), (G) and (H), error bars = s.e.m.

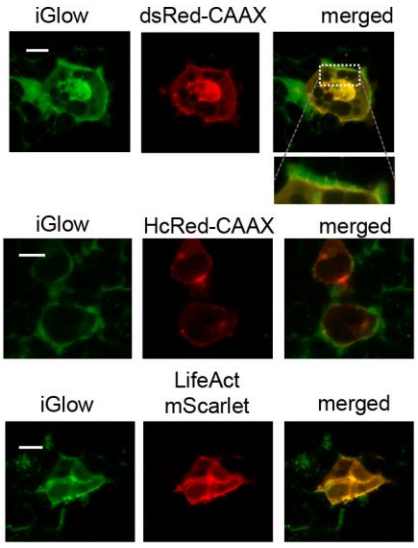

Figure 2: Confocal imaging of iGlow expressing cells. Live-cell confocal images of cells co-expressing iGlow and dsRed-CAAX (top), HcRed-CAAX (middle), or LifeAct-mScarlet (bottom). In all panels, horizontal bars = 10 µm.

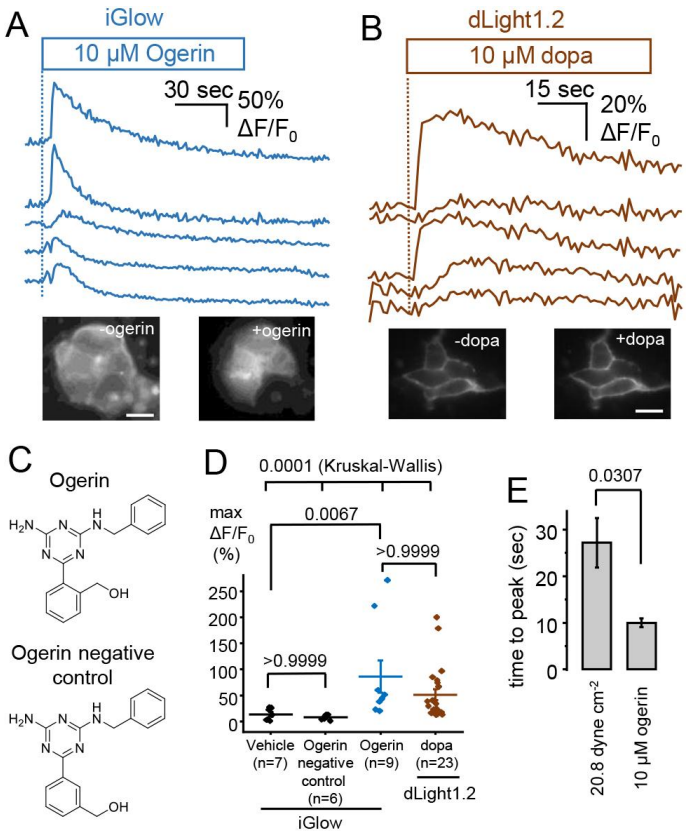

Figure 3: Chemical activation of iGlow with Ogerin. (**A**) *Top*: Fluorescence time-course of iGlow expressing cells in response to acute perfusion with 10 µM Ogerin. *Bottom*: images of cells before and after Ogerin perfusion. (**B**) *Top*: Fluorescence time-course of dLight1.2 expressing cells in response to acute perfusion with 10 µM dopamine (dopa). *Bottom*: images of cells before and after dopamine perfusion. (**C**) Chemical structures of Ogerin and its inactive analog generated using ChemDraw. (**D**) Scatter plots showing max $\Delta F/F_0$ values obtained from iGlow expressing cells acutely perfused with 10 µM Ogerin (blue dots, n = 9), a vehicle control (n = 7), or 10 µM of the inactive Ogerin analog (n = 6). The plot also shows max $\Delta F/F_0$ values obtained from dLight1.2 expressing cells acutely perfused with 10 µM dopamine (brown dots, n = 20). Numbers above plots indicate p-values from Dunn's multiple comparisons tests and one-

way Kruskal-Wallis analysis of variance. (**E**) Comparison of time to peak values obtained from iGlow expressing cells exposed to a high amplitude shear stress pulse or 10 µM Ogerin. Numbers above plots indicate p-values from a Mann Whitney U-test. In panels (A) and (B), horizontal bars = 10 µm. In panels (D) and (E), error bars = s.e.m.

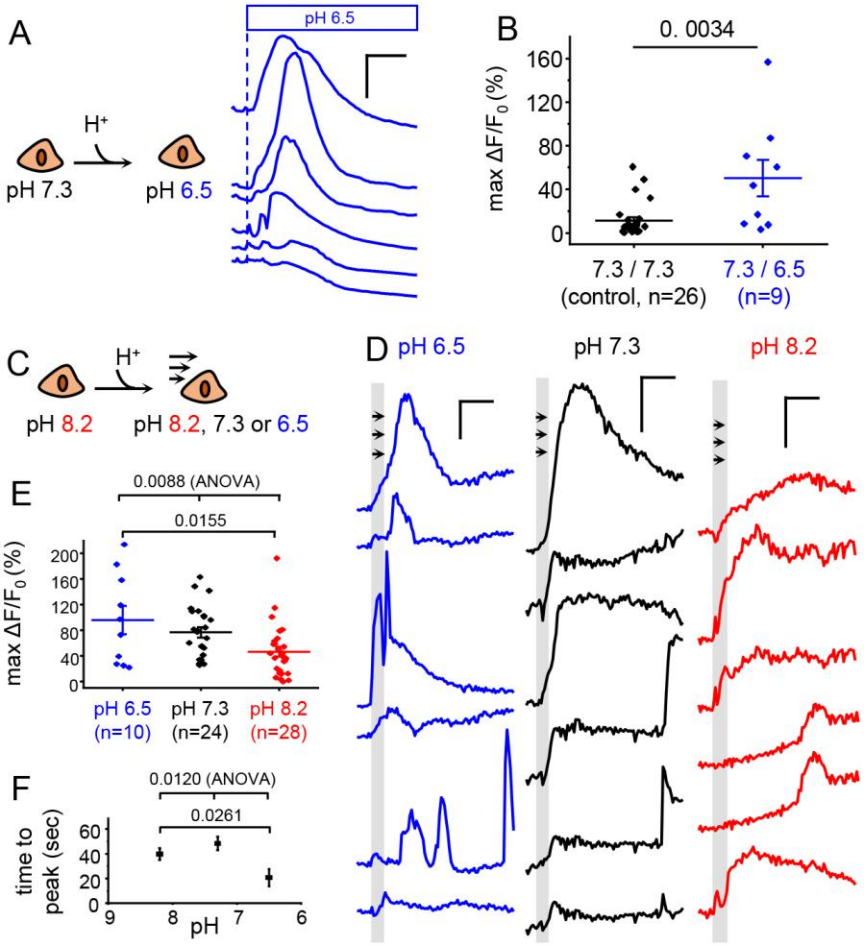

Figure 4: Modulation of iGlow signals by extracellular pH. (**A**) Examples of fluorescence time course from individual iGlow-expressing cells exposed to acute extracellular acidification from pH 7.3 to pH 6.5. (**B**) Scatter plots showing max $\Delta F/F_0$ values from data obtained from (A) (7.3 / 6.5, n = 9) and from control experiments with no pH change (7.3 / 7.3, n = 26). Numbers above plots indicate p-value from a Mann Whitney U-test. (**C**) iGlow expressing cells were incubated at pH 8.2 and exposed to a single shear stress pulse using extracellular solution of indicated pH. (**D**) Representative fluorescence time course of single iGlow-expressing cells from experiment depicted in (C). Vertical bars = 50% $\Delta F/F_0$, horizontal bars = 20 sec. (**E**) Scatter

plots showing max $\Delta F/F_0$ values from experiments depicted in (C). Numbers above plots indicate p-values from Tukey's multiple comparisons tests and one-way ANOVA. (**F**) Plot showing the mean time to peak values as function of extracellular pH from data shown in (E). Numbers above plots indicate p-values from Tukey's multiple comparisons tests and one-way ANOVA. In (B), (E), and (F), error bars = s.e.m.

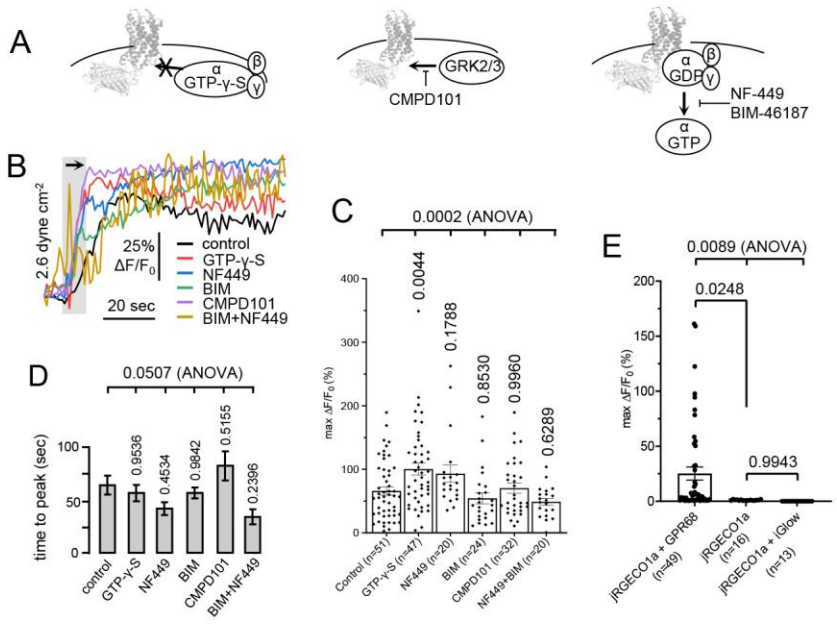

Figure 5: Flow-induced iGlow signals are not abolished by pharmacological modulation of downstream G-protein signaling. (**A**) Expected effects of pharmacological treatments on protein-protein interactions between iGlow, Gα proteins and GRK2/3 kinases. (**B**) Representative fluorescence time-course of iGlow-expressing cells treated with 0.2 mM GTP-γ-S (red trace), 20 µM NF-449 (blue trace), 20 µM BIM-46187 (BIM, green trace), 10 µM CMPD101 (purple trace) or a vehicle control (black trace) and exposed to an acute shear stress pulse. (**C**) Scatter plots showing the max $\Delta F/F_0$ values obtained following shear stress stimulation in cells treated with GTP-γ-S (n = 33), NF-449 (n = 20), BIM-46187 (BIM, n = 21), CMPD101 (n = 17) or a vehicle control (n =25). (**D**) Histograms showing the mean time to peak values from data obtained in (C). **(E)** Scatter plots showing calcium-sensitive fluorescence signals obtained by decreasing extracellular pH from 7.3 to 6.5 in cells transfected with the red calcium indicator jRGECO1a and co-transfected or not with a plasmid encoding wild-type GPR68 or iGlow. Numbers above plots in (C), (D), and (E) indicate p-values from Dunnett's multiple comparisons tests and one-way ANOVA. Error bars = s.e.m.

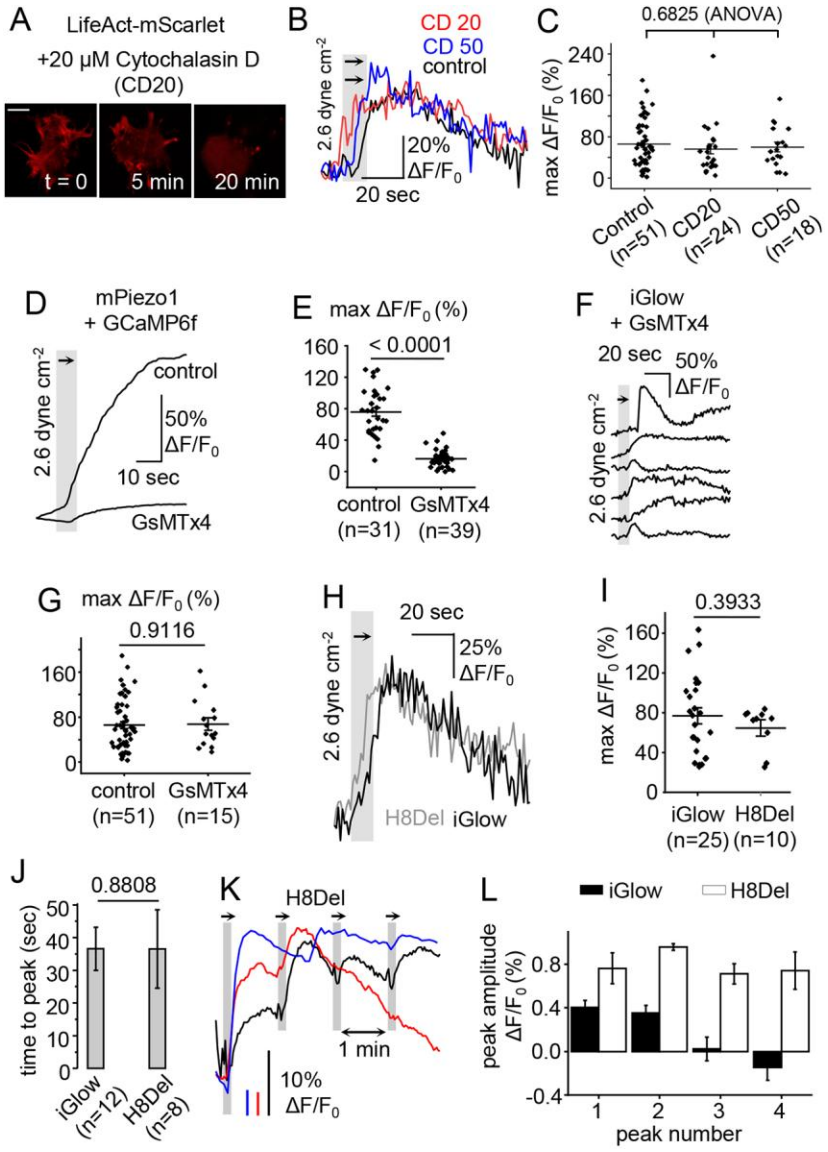

Figure 6: Flow-induced iGlow signals are not abolished by experimental manipulations known to modulate mechanosensitivity in ion channels and GPCRS. (**A**) Confocal images of a LifeAct-mScarlet-expressing cell at indicated times following incubation with 20 µM Cytochalasin D (CD) (scale bar = 10 µm). (**B**) Representative fluorescence time-course of iGlow from cells incubated for 20 min with 20 µM CD (red), 50 µM CD (blue) or a control solution (black) and exposed to a shear stress pulse. (**C**) Scatter plots showing max $\Delta F/F_0$ values from

experiments depicted in (B). (**D**) Example of calcium sensitive fluorescence time-course of cells co-expressing PIEZO1 and GCaMP6f in presence (blue trace) or absence (black trace) of 2.5 µM GsMTx4 and exposed to a shear stress pulse. (**E**) Scatter plots showing max $\Delta F/F_0$ values obtained from experiments depicted in (D). (**F**) Examples of iGlow fluorescence time course in presence of 2.5 µM GsMTx4. (**G**) Scatter plots showing max $\Delta F/F_0$ values obtained from (F). (**H**) Representative fluorescence traces from iGlow and H8del. (**I**) Scatter plots showing max $\Delta F/F_0$ values from experiments shown in (H). (**J**) Histogram comparing time to peak values between iGlow and H8Del from experiments depicted in (H-I). (**K**) Fluorescence time course from H8Del expressing cells obtained with repeated shear stress pulse (1.7 dyne cm^{-2}) with 1 min recovery. (**L**) Peak amplitude of fluorescence signals produced by iGlow (solid bars) and H8Del (open bars) as function of peak number (n = 3). Numbers above plots indicate p-values from one-way ANOVA (C), Student's T-tests ((E), (G), (I)), or Mann-Whitney U test (J). In (C), (E), (G), (I), (J), and (L), error bars = s.e.m.

ATGGGGAACATCACTGCAGACAACTCCTCGATGAGCTGTACCATCGACCATACCATCCACCAGACGCTG
GCCCCGGTGGTCTATGTTACCGTGCTGGTGGTGGGCTTCCCGGCCAACTGCCTGTCCCTCTACTTCGGC
TACCTGCAGATCAAGGCCCGGAACGAGCTGGGCGTGTACCTGTGCAACCTGACGGTGGCCGACCTCTTC
TACATCTGCTCGCTGCCCTTCTGGCTGCAGTACGTGCTGCAGCACGACAACTGGTCTCACGGCGACCTG
TCCTGCCAGGTGTGCGGCATCCTCCTGTACGAGAACATCTACATCAGCGTGGGCTTCCTCTGCTGCATC
TCCGTGGACCGCTACCTGGCTGTGGCCCATCCCTTCCGCTTCCACCAGTTCCGGACCCTGAAGGCGGCC
GTCGGCGTCAGCGTGGTCATCTGGGCCAAGGAGCTGCTGACCAGCATCTACTTCCTGATGCACGAGGAG
GTCATCGAGGACGAGAACCAGCACCGCGTGTGCTTTGAGCACTACCCCATCCAGGCATGGCAGCGCGCC
ATCAACTACTACCGCTTCCTGGTGGGCTTCCTCTTCCCCATCTGCCTGCTGCTGGCGTCCTACCAGGGC
ATCCTGCGCGCCGTGCGCCGGAGCCTGAGCTCACTCATTAACGTCTATATCAAGGCCGACAAGCAGAAG
AACGGCATCAAGGCGAACTTCAAGATCCGCCACAACATCGAGGACGGCGGCGTGCAGCTCGCCTACCAC
TACCAGCAGAACACCCCCATCGGCGACGGCCCCGTGCTGCTGCCCGACAACCACTACCTGAGCGTGCAG
TCCAAACTTTCGAAAGACCCCAACGAGAAGCGCGATCACATGGTCCTGCTGGAGTTCGTGACCGCCGCC
GGGATCACTCTCGGCATGGACGAGCTGTACAAGGGCGGTACCGGAGGGAGCATGGTGAGCAAGGGCGAG
GAGCTGTTCACCGGGGTGGTGCCCATCCTGGTCGAGCTGGACGGCGACGTAAACGGCCACAAGTTCAGC
GTGTCCGGCGAGGGTGAGGGCGATGCCACCTACGGCAAGCTGACCCTGAAGTTCATCTGCACCACCGGC
AAGCTGCCCGTGCCCTGGCCCACCCTCGTGACCACCCTGACCTACGGCGTGCAGTGCTTCAGCCGCTAC
CCCGACCACATGAAGCAGCACGACTTCTTCAAGTCCGCCATGCCCGAAGGCTACATCCAGGAGCGCACC
ATCTTCTTCAAGGACGACGGCAACTACAAGACCCGCGCCGAGGTGAAGTTCGAGGGCGACACCCTGGTG
AACCGCATCGAGCTGAAGGGCATCGACTTCAAGGAGGACGGCAACATCCTGGGGCACAAGCTGGAGTAC
AACAATCATGACCAACTGAGCCGCAAGGACCAGATCCAGCGGCTGGTGCTCAGCACCGTGGTCATCTTC
CTGGCCTGCTTCCTGCCCTACCACGTGTTGCTGCTGGTGCGCAGCGTCTGGGAGGCCAGCTGCGACTTC
GCCAAGGGCGTTTTCAACGCCTACCACTTCTCCCTCCTGCTCACCAGCTTCAACTGCGTCGCCGACCCC
GTGCTCTACTGCTTCGTCAGCGAGACCACCCACCGGGACCTGGCCCGCCTCCGCGGGGCCTGCCTGGCC
TTCCTCACCTGCTCCAGGACCGGCCGGGCCAGGGAGGCCTACCCGCTGGGTGCCCCCGAGGCCTCCGGG
AAAAGCGGGGCCCAGGGTGAGGAGCCCGAGCTGTTGACCAAGCTCCACCCGGCCTTCCAGACCCCTAAC
TCGCCAGGGTCGGGCGGGTTCCCCACGGGCAGG

MGNITADNSSMSCTIDHTIHQTLAPVVYVTVLVVGFPANCLSLYFGYLQIKARNELGVYLCNLTVADLF
YICSLPFWLQYVLQHDNWSHGDLSCQVCGILLYENIYISVGFLCCISVDRYLAVAHPFRFHQFRTLKAA
VGVSVVIWAKELLTSIYFLMHEEVIEDENQHRVCFEHYPIQAWQRAINYYRFLVGFLFPICLLLASYQG
ILRAVRRSLSSLINVYIKADKQKNGIKANFKIRHNIEDGGVQLAYHYQQNTPIGDGPVLLPDNHYLSVQ
SKLSKDPNEKRDHMVLLEFVTAAGITLGMDELYKGGTGGSMVSKGEELFTGVVPILVELDGDVNGHKFS
VSGEGEGDATYGKLTLKFICTTGKLPVPWPTLVTTLTYGVQCFSRYPDHMKQHDFFKSAMPEGYIQERT
IFFKDDGNYKTRAEVKFEGDTLVNRIELKGIDFKEDGNILGHKLEYNNHDQLSRKDQIQRLVLSTVVIF
LACFLPYHVLLLVRSVWEASCDFAKGVFNAYHFSLLLTSFNCVADPVLYCF[VSETTHRDLARLRGACL
AFLTCSRTGRAREAYPLGAPEASGKSGAQGEEPELLTKLHPAFQTPNSPGSGGFPTGR]

Fig. S1. Nucleic acid (top) and amino acids (bottom) sequences of iGlow.

Black = GPR68; purple = linkers; green = cpGFP; red = Helix 8. Brackets indicate the C-terminal fragment eliminated in H8Del.

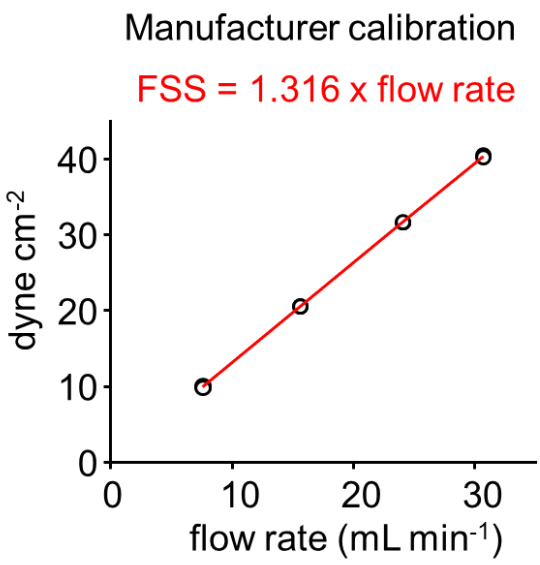

Fig. S2. Shear stress calibration. Shear stress applied through our flow chamber was calculated using the manufacturer's calibration.

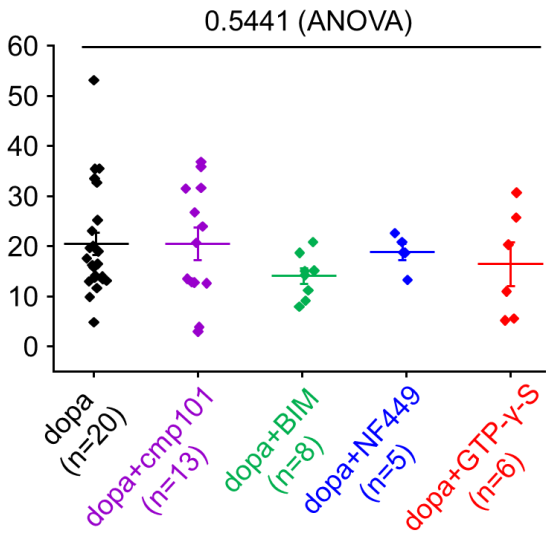

Fig. S3. Dopamine sensitivity of dLight1.2 is not eliminated by pharmacological modulation of G protein signaling. The scatter plots show max $\Delta F/F_0$ values obtained upon acute perfusion with 10 µM dopamine in cells pre-treated with CMPD101 (purple dots, n = 13), BIM-46187 (BIM, green dots, n = 8), NF-449 (blue dots, n = 5), GTP-γ-S (red dots, n = 6), or a vehicle control (black dots, n = 20). The number above the graph indicates the exact p-value from a one-way ANOVA. Error bars = s.e.m.

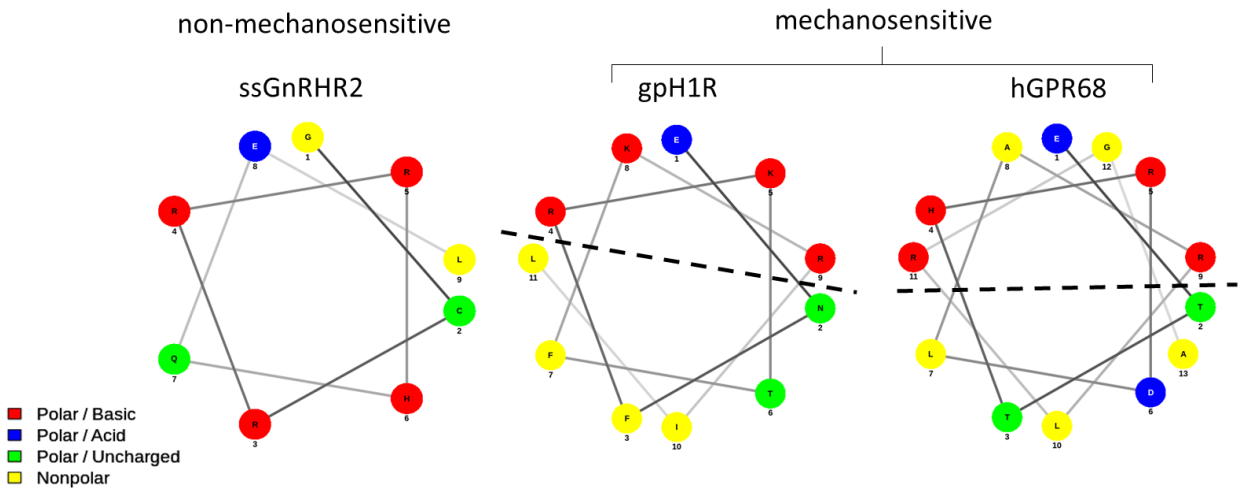

Fig. S4. Prediction of an amphipathic Helix 8 in GPR68 using the online predictor NetWheels. Helical wheel plot of Helix 8 in the long isoform of the swine gonadotropin-releasing hormone receptor (ssGnRHR2), the guinea pig histamine H1 receptor (gpH1R) and human GPR68 (hGPR68). The dotted line indicates the separation between the polar vs. apolar interfaces of the Helix.

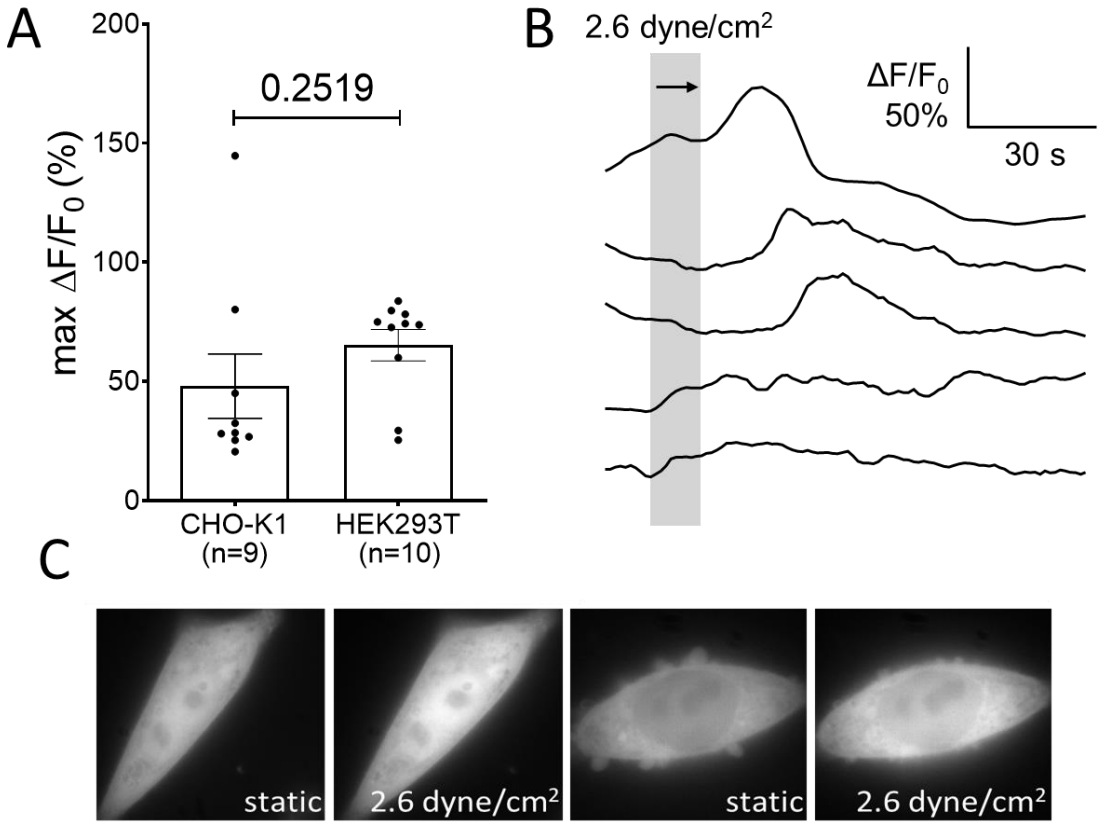

Fig. S5. H8Del is functionally expressed in CHO-K1 cells. (A) Scatter plots showing maximum $\Delta F/F_0$ in CHO-K1 and HEK293-ΔPz1 cells transfected with H8Del and exposed to 2.6 dyne cm^{-2} of shear stress for 10 sec. (B) Representative time-course traces of individual cells. The duration of shear stimulus is indicated in grey. (C) Epifluorescence images of CHO-K1 cells before and after shear stimulus.

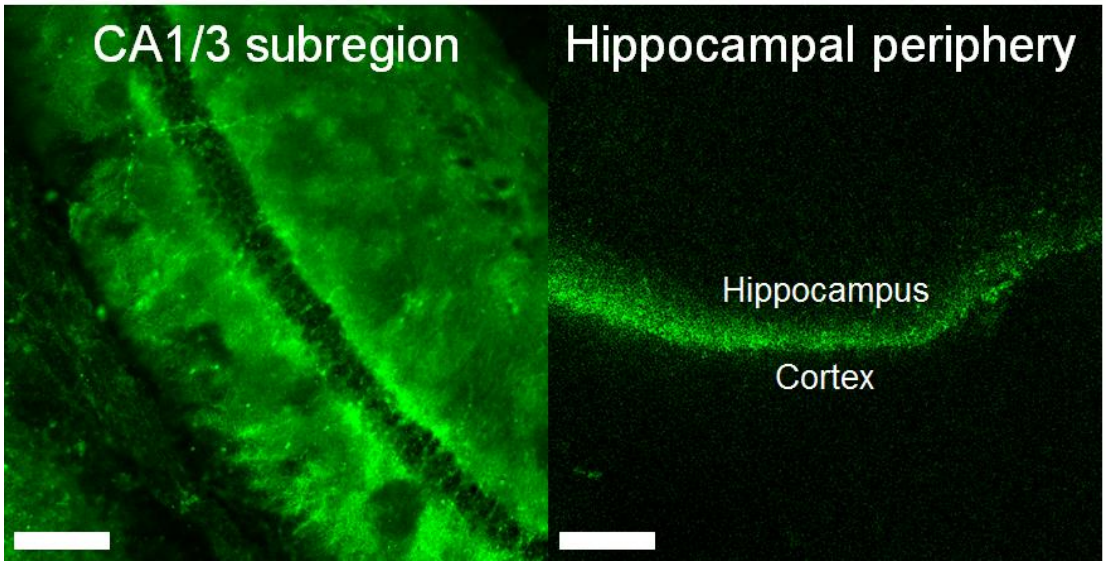

Fig. S6. AAV-mediated expression of iGlow in mouse hippocampal CA3 region. Confocal microscopy images at the site of injection (CA1/3 subregion) and its surrounding (Hippocampal periphery). The faint peripheral signal is produced by background autofluorescence. Scale bars = 150 µM.

Table S1. Primers used to insert cpGFP into GPR68 using High-Fidelity DNA assembly.

primers	**Sequences (5'→3')**
GPR68 Fwd (backbone)	aatcatgaccaactgagccgcaaggaccagatccagcgg
GPR68 Rev (backbone)	aatgagtgagctcaggctccggcgcacggcgcg
cpGFP with linkers Fwd	gcgccggagcctgagctcactcattaacgtctatatcaaggcc
cpGFP with linkers Rev	ccttgcggctcagttggtcatgattgttgtactccagcttgtg